SOME EFFECTS OF PARTICLE SHAPE ON THE MECHANICAL BEHAVIOUR OF GRANULAR MATERIALS

John Harkness[1] **and Antonis Zervos**[1]

[1] Department of Civil, Maritime and Environmental Engineering
University of Southampton, SO17 1BJ, U.K
J.Harkness@soton.ac.uk

Keywords granular materials; railway ballast; DEM analysis; particle shape

Abstract The behaviour of a granular material depends on the shape, material properties and packing of the grains. Starting with a particle characterization, the ability to make predictions of the macroscopic behaviour of an assembly of particles without recourse to laboratory or numerical experiments would be very useful. With this ultimate goal in mind, this work presents some first findings of an investigation into the effects on macroscopic behaviour of two key measures of particle shape: form and angularity. The form of a particle is quantified using the Longest (L), Intermediate (I) and Shortest (S) dimensions of an equivalent scalene ellipsoid; A sum of the local volumetric deviations of the particle from that ellipsoid as a ratio of the ellipsoid volume is used as a measure of angularity. Discrete element, periodic cell simulations of ellipsoidal and realistic particle shapes sampled from railway ballast are used to investigate mechanical behaviour in terms of critical state friction angle. Characterization of the observed behaviour in terms of a single shape parameter is explored. It is found that deviation of particle form from that of a sphere together with increases in angularity both lead to higher angles of friction at critical state. It is argued that, at least to some extent, the higher critical state strength exhibited by non-spherical particles is due to their form and/or angularity suppressing particle rotation and leading to increased interparticle sliding, a mechanism that in comparison expends more energy.

1 INTRODUCTION

Particle shape is a fundamental property of a granular material. It is quantified by considering three different aspects of shape, which generally correspond to different scales of observation and are assumed independent: particle *form*, *angularity* and *roughness*. Form quantifies the overall shape, angularity is usually considered to describe the number and sharpness of angles on the particle's surface, and roughness relates to the microscopic variations of the particle surface that are to some extent responsible for interparticle friction. Form in particular is generally quantified using the longest (L), intermediate (I) and

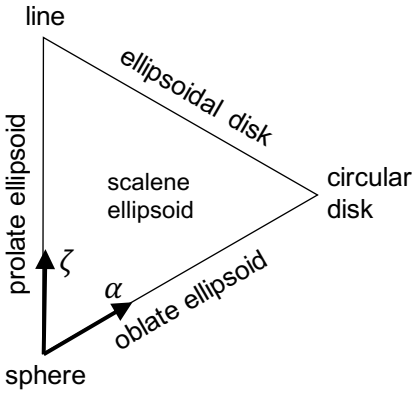

Figure 1: The platyness $\alpha = 2(I - S)/(L + I + S)$ vs. elongation $\zeta = (L - I)/(L + I + S)$ space, with a description of the corresponding forms.

shortest (S) dimensions of the particle along orthogonal axes. Whilst different measures of form have been proposed, no consensus exists on whether one has an advantage over the others [2].

Following the idea first presented in [3], we describe form on the basis of an equivalent scalene ellipsoid, here considered to be the ellipsoid that best fits, in the least squares sense, the shape of the particle. Its axes are taken to represent the dimensions S, I and L. We adopt the framework of [6, 7, 8], where particle form is uniquely defined by two parameters:

$$\alpha = \frac{2(I - S)}{L + I + S}, \qquad \zeta = \frac{L - I}{L + I + S} \tag{1}$$

with $0 \leq \alpha \leq 1$ and $0 \leq \zeta \leq 1$.

All possible ellipsoids plot in $\alpha - \zeta$ space within the triangle of Figure 1. In a further departure from customary practice, we define as *angularity* the sum of the local volumetric deviations of the particle's shape from its equivalent scalene ellipsoid, divided by the ellipsoid's volume [5].

To investigate the effect of these three measures, we perform DEM simulations of triaxial compression (employing periodic boundaries) on granular assemblies representative of ballast particles. We use the method of potential particles [4], which allows modelling of (almost) arbitrary shapes.

To investigate the effect of these three measures, we perform DEM simulations of triaxial compression (employing periodic boundaries) on granular assemblies representative of ballast particles. We use the method of potential particles [4], which allows modelling of (almost) arbitrary shapes.

2 METHOD

Discrete element, periodic cell models were created, each using particles of a single form and angularity. The particle size distribution (PSD) was the same for each model and was representative of railway ballast as defined in [1] and shown in Table 1, in each case keeping the intermediate dimensions, I, equal to the respective sieve size. The number of particles for each different form was chosen (by trial and error) such that the longest dimension of the largest particle did not exceed a quarter of the shortest dimension of cell (with the particles in their densest state); this condition was easily satisfied for the spherical forms with about 4000 particles, but up to about 65,000 were required for the most elongated shapes. To create a specimen, particles were randomly dispersed and oriented within a cell of relative dimensions of 1:1:2 (width:depth:height) to a target initial void ratio of 2.0. The model was then subjected to isotropic compression with zero gravity and zero inter-particle friction. Once a void ratio of 0.65 was reached, an isotropic stress of 100 kPa was applied to the boundaries and the model was allowed to reach equilibrium. At that point inter-particle friction was reintroduced and the model was subjected to triaxial loading, where the lateral boundaries were stress controlled at 100 kPa and the top boundary moved downwards at a constant velocity (set to 0.076 of the initial height of the cell). Table 2 shows the model parameters with Hertzian contacts used for all the tests in this paper.

Table 1: Particle size distribution for modelled particles

Sieve Size (mm)	28.5	36.5	40.5	46	52
Passing by Mass (%)	10	30	50	70	90

Table 2: Material Properties

Properties	Value
Particle Density	2700 kg/m^3
Interparticle Friction Angle	30°
Particle Young's Modulus	40 GPa
Particle Poison's Ratio	0.3

Two sets of simulations were carried out: the first with a wide range of forms (presented in Table 3) using ellipsoidal particles (zero angularity); the second with constant form, but varying angularity. For the latter set, four particles, spanning the range of forms for a measured railway ballast, were selected and for each, a range of new numerical particles was then created, interpolating between the scanned particle and its equivalent scalene ellipsoid, as discussed below.

Form	Platyness α	Elongation ζ	L : I : S
1	0.0	0.0	1:1:1
2	0.0	0.1	1:1:1.3333
3	0.0	0.2	1:1:1.75
4	0.0	0.3	1:1:2.2857
5	0.0	0.4	1:1:3
6	0.0	0.5	1:1:4
7	0.0	0.6	1:1:5.5
8	0.1	0.0	0.8571:1:1
9	0.1	0.1	0.8421:1:1.3158
10	0.1	0.2	0.8235:1:1.7059
11	0.1	0.3	0.8:1:2.2
12	0.1	0.4	0.7692:1:2.8462
13	0.1	0.5	0.7273:1:3.7273
14	0.2	0.0	0.7273:1:1
15	0.2	0.1	0.7:1:1.3
16	0.2	0.2	0.6667:1:1.6667
17	0.2	0.3	0.625:1:2.125
18	0.2	0.4	0.5714:1:2.7143
19	0.3	0.0	0.6087:1:1
20	0.3	0.1	0.5714:1:1.2857
21	0.3	0.2	0.5263:1:1.6316
22	0.3	0.3	0.4706:1:2.0588
23	0.3	0.4	0.4:1:2.6
24	0.4	0.0	0.5:1:1
25	0.4	0.1	0.4545:1:1.2727
26	0.4	0.2	0.4:1:1.6
27	0.4	0.3	0.3333:1:2
28	0.5	0.0	0.4:1:1
29	0.5	0.1	0.3478:1:1.2609
30	0.5	0.2	0.2857:1:1.5714
31	0.6	0.0	0.3077:1:1
32	0.6	0.1	0.25:1:1.25
33	0.7	0.0	0.2222:1:1
34	0.7	0.1	0.16:1:1.24
35	0.8	0.0	0.1429:1:1

Table 3: Table of ellipsoid forms considered in the analyses.

2.1 Varying angularity with constant form

For this analysis, four particles were selected from a library of scanned ballast particles, corresponding to the most spherical, an average form and the two extremes of elongation

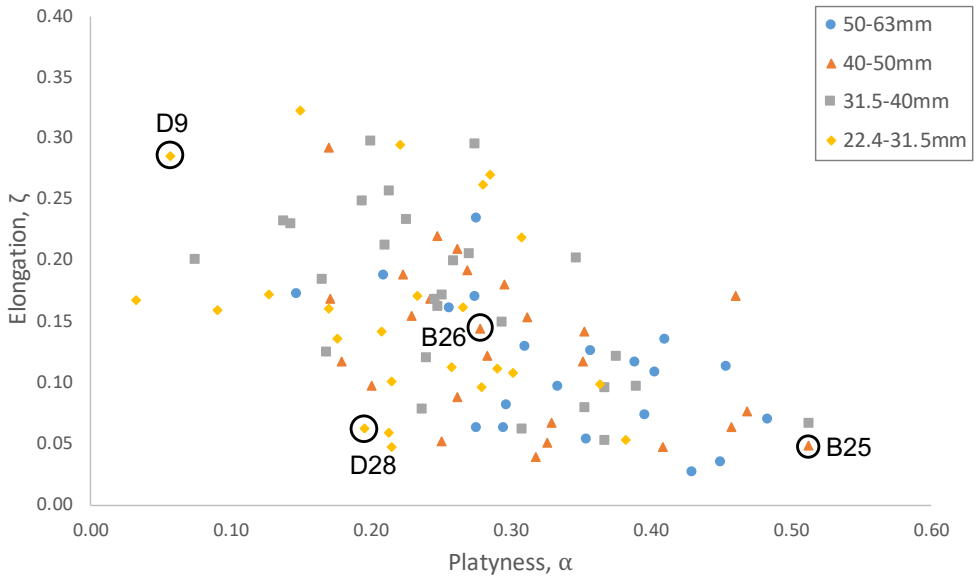

Figure 2: Plot of ballast forms for scanned ballast particles.

and platyness. Figure 2 shows the distribution of ballast forms in the library together with the particles identified for further analysis. To investigate the variation of angularity with constant form, an equivalent scalene ellipsoid was fitted to each of the particle surface meshes through minimization of the sum of the squares of the distances from each vertex (of the surface mesh) to its nearest point on the ellipsoid. A particle's angularity is then calculated as the sum of the local volumetric deviations of the particle's shape from its equivalent scalene ellipsoid, divided by the ellipsoid's volume [5].

For a particle, the location of each surface mesh vertex, V_p, can be written as a sum of the projection of each vertex onto the surface of the fitted ellipsoid, V_e, and a displacement vector, V_{ep} as:

$$V_p = V_e + sV_{ep} \tag{2}$$

with s as a scale parameter. When $s = 1$, the particle is recreated in its original shape. However, varying s (for $0 <= s <= 1$) allows for an interpolation of the shape between its equivalent scalene ellipsoid and the original particle shape. For a projection of the surface vertices to the nearest points on the best-fit ellipsoid (such that each vector V_{ep} is orthogonal to the ellipsoid surface at the point V_e), the nearest point from V_p to the ellipsoid surface will remain unchanged (V_e) for different values of s. Thus the best-fit ellipsoid is also unchanged and the form of the interpolated particle is therefore constant with s, while the angularity (as defined here) increases with s. For $s > 1$, it is possible to extrapolate (to some extent) to form a particle with angularity greater than that of the original scanned particle. This process is illustrated in Figure 3.

To model the new particles as discrete elements, overlapping clumps of between 100 and 1000 spheres were used, an example of which is presented in Figure 4. As these shapes are not perfect representations of their mesh counterparts, the form and angularity were calculated again for the clumped-sphere representations. The parameters for the clumped-sphere particles tested are shown in Table 4. The variations for each particle scan are presented together in the table for values of s from 0 to 1.5. It can be seen that the platyness and elongation remain fairly constant for variations in angularity of each particle.

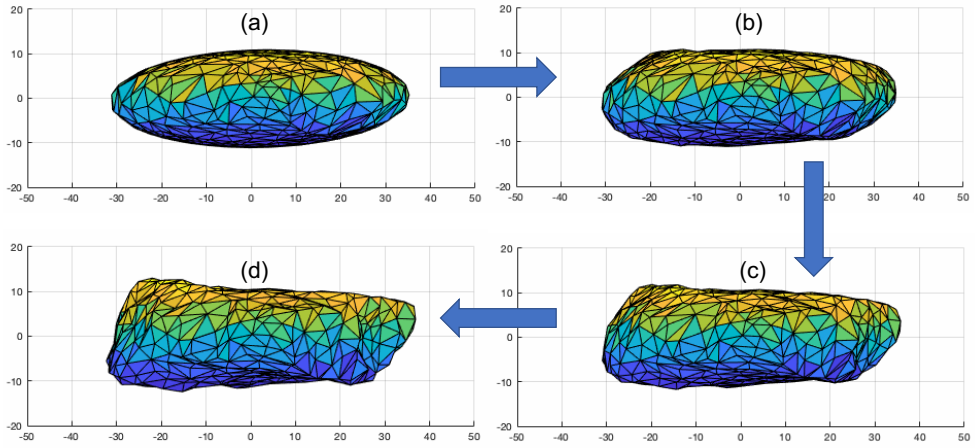

Figure 3: Varying angularity with constant form for a ballast particle.

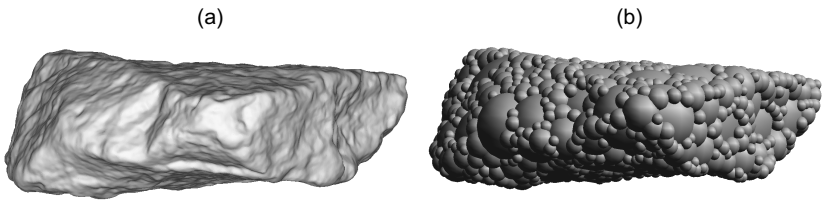

Figure 4: A ballast particle scan and its representation with 1000 clumped spheres.

3 RESULTS

Figure 5 presents a plot of friction angle at critical state ϕ'_{crit} as a function of particle platyness and elongation. Each point represents the result of a model consisting of ellipsoids with the corresponding form. The results can be fitted reasonably accurately by a plane, which is also plotted, showing that ϕ'_{crit} varies linearly with α and ζ. Evidently ϕ'_{crit} depends on a single parameter, corresponding to the distance along the direction of the maximum gradient of this plane. This parameter is equal to

Particle name	Angularity	Platyness α	Elongation ζ	Number of spheres
100-B25-0	0.0293	0.5503	0.0296	100
100-B25-1	0.1137	0.5527	0.0248	100
100-B25-2	0.2116	0.5545	0.0249	100
100-B25-3	0.3036	0.5732	0.0107	100
1000-B25-0	0.0130	0.5417	0.0286	1000
1000-B25-3	0.3192	0.5705	0.0035	1000
100-B26-0	0.0281	0.2840	0.1583	100
100-B26-1	0.1381	0.2885	0.1518	100
100-B26-2	0.2685	0.2817	0.1619	100
100-B26-3	0.3873	0.2998	0.1415	100
1000-B26-0	0.0136	0.2835	0.1522	1000
1000-B26-3	0.3844	0.2878	0.1441	1000
100-D9-0	0.0385	0.1181	0.3311	100
100-D9-1	0.1607	0.1068	0.3308	100
100-D9-2	0.2936	0.1095	0.3308	100
100-D9-3	0.4243	0.1251	0.3280	100
1000-D9-0	0.0130	0.1076	0.3283	1000
1000-D9-3	0.4290	0.1315	0.3156	1000
100-D28-0	0.0307	0.2976	0.0428	100
100-D28-1	0.1462	0.3028	0.0408	100
100-D28-2	0.2809	0.3050	0.0323	100
100-D28-3	0.3977	0.3052	0.0335	100
1000-D28-0	0.0117	0.2935	0.0433	1000
1000-D28-3	0.3928	0.2702	0.0423	1000

Table 4: Table of interpolated forms with varying angularity and approximately constant form. The particle names are composed as: (N-ID-X), where N is the number of spheres used, ID is the scanned particle identifier and $X = 2s$ and where s is the scaling factor from equation 2.

$F' = (1.0166 \cdot L - 0.0333 \cdot I - 0.9834 \cdot S)/(L+I+S)$ or, acknowledging that the contribution of I is very small compared to the contributions of L and S, which are practically equal:

$$F = \frac{L - S}{L + I + S} \tag{3}$$

We call the parameter defined by equation 3 the *effective form* of a particle, in the sense that it suffices to predict (at least for ellipsoidal particles) the strength of the aggregate. Figure 5 shows a plot of ϕ'_{crit} vs F, along with the linear best fit and the 95% confidence intervals, demonstrating a tight correlation where ϕ'_{crit} is predicted within $\pm 1°$.

Figure 6 shows the friction angle at critical state plotted against the angularity and the effective form, F, for the clumped-sphere particles together with the ellipsoid data

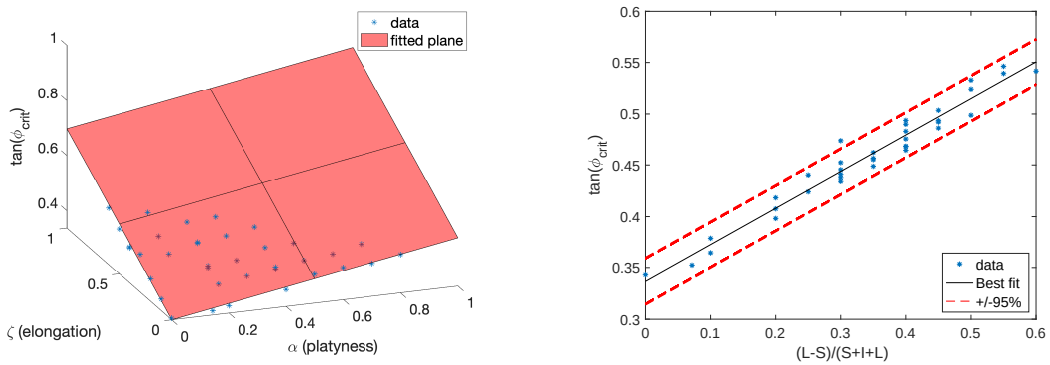

Figure 5: Friction angle at critical state for ellipsoidal particles, as a function of: particle platyness α and elongation ζ (left); effective form F (right).

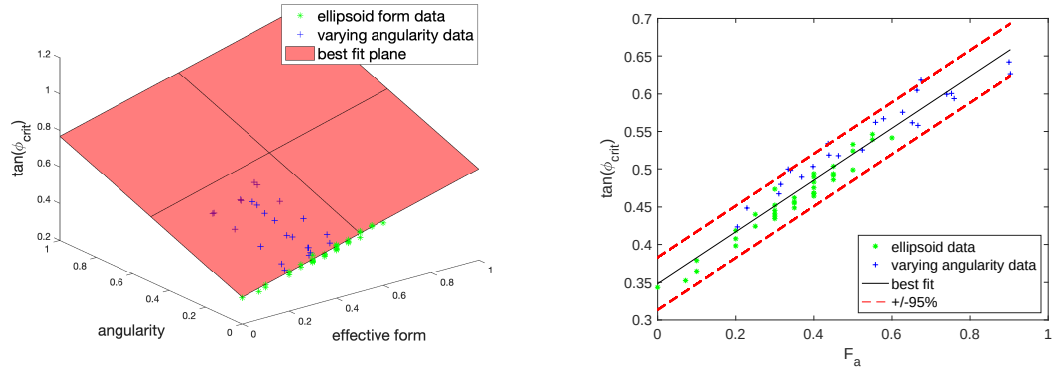

Figure 6: Friction angle at critical state for both sets of particles, as a function of: angularity and effective form (left); angularity-augmented effective form F_a (right).

from Figure 5. Once again, a plane can be fitted reasonably well to the data and a further parameter can be defined as $F_a = F + 1.21 \times \text{angularity} \approx F + (6/5) \times \text{angularity}$, corresponding to the distance along the maximum gradient of the plane. Figure 6 shows a plot of ϕ'_{crit} vs the angularity-augmented effective form, F_a, along with the linear best fit and the 95% confidence intervals, demonstrating a similarly tight correlation between strength and F_a, with ϕ'_{crit} predicted within $\pm 1.5°$.

As already shown in [6, 7, 8] for some of the models also presented here, the higher ϕ'_{crit} exhibited by non-spherical and/or angular particles is due to their form and/or angularity suppressing particle rotation and leading to increased interparticle sliding, a mechanism that in comparison expends more energy.

3.1 Particle rotation and sliding

To examine further the trends in particle behaviour at critical state as a function of particle form, particle rotation and sliding at contacts were investigated. The particle

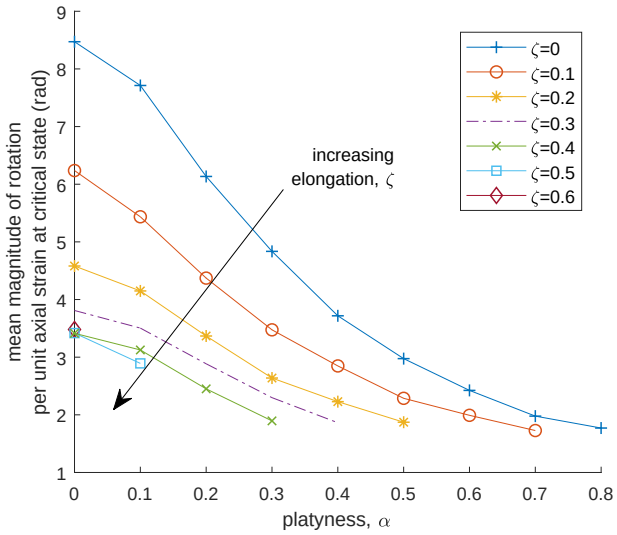

Figure 7: Average magnitude of particle rotation per unit axial strain at critical state.

rotations were calculated by finding the relative orientations of particles between adjacent model states, saved every $\approx 1\%$ axial strain. The magnitudes of the rotations were then averaged for all particles and normalized by the axial strain for each saved state and over all states in the critical state zone.

The average particle rotation per unit axial strain is plotted against platyness for all of the ellipsoidal forms in Figure 7. Additionally, the ratio of contacts sliding (averaged over the saved states in the critical state zone) is presented in Figure 8.

Figures 7 and 8 show a clear reduction in average particle rotation and an equally clear increase in sliding ratio with increasing platyness (α) and elongation (ζ) for all apart from the highest values of α and ζ. This is consistent with the higher friction angles observed with the less spherical particles: less able to roll over each other and needing instead to slide.

However, at higher values of both α and ζ, the reduction in rotation and increase in sliding appear to plateau. This can also be seen in the sliding behaviour in Figure 8: in this case the ratio of sliding contacts mostly increases with increasing α and ζ, although this trend levels off for high α and ζ and even goes into reverse for high values of platyness. One possible explanation is that particles with more extreme aspect ratios tend to clump together, effectively forming a more spherical agglomeration and permitting a more efficient deformation mechanism for the particle assembly.

4 CONCLUSIONS

Discrete element simulations were used to investigate the dependence of the friction angle at critical state, ϕ_{crit}, on the form and angularity of particles. Simulations with ellipsoids showed a very strong correlation between ϕ_{crit} and a single parameter of effec-

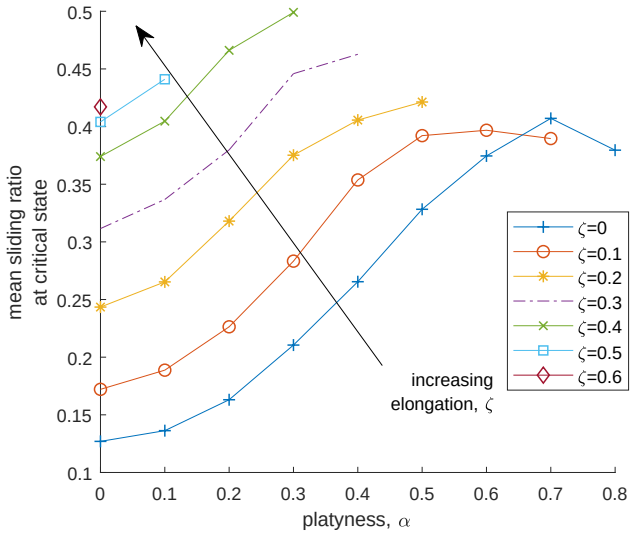

Figure 8: Average ratio of sliding to non-sliding contacts at critical state.

tive form, approximated by $(L-I)/(S+I+L)$ (in which S, I and L are the shortest, intermediate and longest dimensions of the ellipsoid). A second set of simulations added increasing angularity to particles of constant form (modelled with clumps of overlapping spheres). The results demonstrated a reasonably linear dependence of ϕ_{crit} with both angularity and effective form, enabling the definition of a single augmented-form parameter, with a strong correlation to ϕ_{crit}. An examination of average particle rotation and sliding ratio for ellipsoidal particles in the critical state showed a clear decrease in rotation and a corresponding increase in sliding ratio for increases in platyness and elongation.

Acknowledgements

We gratefully acknowledge support from Network Rail through its Strategic Partnership with the University of Southampton, and from the E.P.S.R.C. Track21 (EP/H044949/1) and Track2Future (EP/M025276/1) Programme Grants. Use of the IRIDIS High Performance Computing Facility and associated support services at Southampton are also acknowledged. Some of the models using ellipsoidal particles presented here were developed by M. Potticary and were first presented in [5, 6, 7, 8].

REFERENCES

[1] *BSI Standards Publication Aggregates for railway ballast BS EN 13450:2013 BSI.* BSI Standards Limited 2013, 2013.

[2] S.J. Blott and K. Pye. Particle shape: a review and new methods of characterization and classification. *Sedimentology*, pages 31–63, September 2007.

[3] C.R.I. Clayton, C.O.R. Abbireddy, and R. Schiebel. A method of estimating the form of coarse particulates. *Géotechnique*, 59(6):493–501, 2009.

[4] J Harkness. Potential particles for the modelling of interlocking media in three dimensions. *International Journal for Numerical Methods in Engineering*, 80:1573–15(June):1573–1594, 2009.

[5] M. Potticary. *A Numerical Investigation of the Effect of Particle Shape on the Strength of Coarse Granular Materials*. PhD Thesis, University of Southampton, 2018.

[6] M. Potticary, A. Zervos, and J. Harkness. A numerical investigation into the effect of particle form on the strength of granular materials. In A. Javadi and M. S. Hussain, editors, *Proceedings of the 22nd UK National Conference of the Association for Computational Mechanics in Engineering*, pages 61–64, 2014.

[7] M. Potticary, A. Zervos, and J. Harkness. An investigation into the effect of particle platyness on the strength of granular materials using the discrete element method. In E. Oñate, M. Bischoff, D.R.J. Owen, and Wriggers P., editors, *IV International Conference on Particle-based Methods. Fundamentals and Applications (PARTICLES 2015)*, pages 767–778, 2015.

[8] M. Potticary, A. Zervos, and J. Harkness. The effect of particle elongation on the strength of granular materials. In *Proceedings of the 24th UK National Conference of the Association for Computational Mechanics in Engineering*, pages 239–242, 2016.